Electrostatic Environment Surrounding the Activation Loop Phosphotyrosine in the Oncoprotein v-Fps†

Barbara Chie Leon, Igor Tsigelny, and Joseph A. Adams*

Department of Pharmacology, University of California, San Diego, La Jolla, California 92093-0506

Received April 24, 2001; Revised Manuscript Received June 25, 2001

ABSTRACT: Autophosphorylation of Tyr-1073 in the activation loop of the oncoprotein v-Fps enhances the phosphoryl transfer reaction without influencing substrate, ATP, or metal ion binding affinities [Saylor, P., et al. (1998) *Biochemistry 37*, 17875−17881]. A structural model of v-Fps, generated from the insulin receptor, indicates that pTyr-1073 chelates two arginines. Mutation of these residues to alanine (R1042A and R1066A) results in weakly phosphorylated enzymes, indicating that one electropositive center is insufficient for attaining maximum loop phosphorylation and concomitant high catalytic activity. While the turnover rate for R1066A is similar to that for a mutant lacking a phosphorylatable residue in the activation loop, the rate for R1042A is 50-fold slower. While solvent perturbation studies suggest that the former is due to a slow phosphoryl transfer step, the latter effect results from a slow conformational change in the mutant, potentially linked to motions in the catalytic loop. Binding of a stoichiometric quantity of Mg^{2+} is essential for ATP binding and catalysis, while binding of an additional Mg^{2+} ion activates further the wild-type enzyme. The affinity of the R1066A enzyme for the second Mg^{2+} ion is 23-fold *higher* than that of the phosphorylated or unphosphorylated form of wild-type v-Fps, with substrate binding unaffected. Conversely, the affinity of R1066A for a substrate mimic lacking a phosphorylation site is 12-fold *higher* than that for the phosphorylated or unphosphorylated form of wild-type v-Fps, with binding of the second Mg^{2+} ion unaffected. A comparison of these enzyme-independent parameters indicates that Arg-1042 and Arg-1066 induce strain in the active site in the repressed form of the enzyme. While this strain is not relieved in the phosphorylated form, the improvements in catalysis in activated v-Fps compensate for reduced metal and substrate binding affinities.

Many protein kinases are activated by phosphorylation of a key polypeptide region in the kinase domain known as the activation loop (*1*). Some protein kinases catalyze this phosphorylation in an autocatalytic step, while others recruit designated protein kinases to conduct this posttranslational modification. Whatever the method, enhancements in catalytic activity can be extraordinary. For example, the activities of PKA, Cdk2, and v-Fps[1] increase by 2−5 orders of magnitude upon activation loop phosphorylation (*2*−*4*). X-ray diffraction studies of a number of protein kinases indicate that two or three positively charged amino acids stabilize the phosphoamino acid and the activation loop (*5*−*9*). The dephosphorylated loops tend to be disordered, while the phosphorylated loops are rigidly fixed by these electropositive residues (*5*, *6*, *10*−*12*). The precise role of the activation loop in controlling catalysis has been widely debated. While several X-ray models suggest that the dephosphorylated activation loop acts as an autoinhibitor prohibiting substrate access, functional studies have not provided universal support for this model. Dephosphorylation of the activation loops in PKA and v-Fps does not enhance substrate binding (*2*, *3*). Furthermore, recent kinetic studies of the insulin receptor kinase (InRK) show that loop phosphorylation increases the level of substrate binding by only 8-fold (*13*). In comparison, loop phosphorylation has a much larger impact on the rates of phosphoryl transfer in PKA, v-Fps, and the InRK (*2*, *3*, *13*), an effect not expected if the loop behaves as a competitor for substrate and/or ATP.

The roles of the electropositive residues in activation loop stabilization and the facilitation of phosphoryl transfer have not been well characterized. The phosphorylation sites within the activation loops are normally distal from the site of phosphoryl group donation, raising questions regarding the mechanism of regulation. It is possible that the electropositive residues may play a role in translating the effects of loop phosphorylation on catalysis. For example, the two electropositive residues (Arg-363 and Arg-387) within the nonreceptor TPK, Lck, are very close to key catalytic residues. Arg-363 is the first residue in the catalytic loop, a short polypeptide segment which contains a conserved catalytic aspartate that forms a hydrogen bond with the hydroxyl of the substrate (*14*). In Lck, Arg-387 is part of the activation loop and is only five residues away from another conserved aspartate (Asp-382) which chelates the essential activating metal ion, Mg^{2+}, in the active site (*14*). The large increases in catalytic efficiency upon activation loop phosphorylation may be the result of changes in the positions of the metal

† This work was supported by NIH Grant CA 75112.

* To whom correspondence should be addressed. Telephone: (858) 822-3360. Fax: (858) 822-3361. E-mail: joeadams@ucsd.edu.

[1] Abbreviations: GST, glutathione *S*-transferase; InRK, kinase domain of the insulin receptor; Mops, 3-(*N*-morpholino)propanesulfonic acid; PKA, cAMP-dependent protein kinase; TPK, tyrosine-specific protein kinase; v-Fps, nonreceptor TPK and transforming agent of the Fujinami sarcoma virus.

10.1021/bi010838e CCC: $20.00
Published on Web 08/02/2001

chelator and/or the catalytic loop aspartate via these positively charged amino acids.

To understand how activating signals are communicated between the phosphorylation site in the activation loop and key elements in the active site of a protein kinase, we replaced two arginines in the kinase domain of the oncoprotein, v-Fps, and studied the effects of these mutations on several biophysical properties. v-Fps is a nonreceptor TPK and is the transforming agent of the Fujinami sarcoma virus (*15*−*17*). As a member of the Fps/Fes family of nonreceptor TPKs, v-Fps is composed of C-terminal SH2 and kinase domains but, unlike the Src family of TPKs, contains no SH3 domain. The viral form differs from the cellular counterpart, c-Fps, by the addition of a gag sequence. The cellular forms of the Fps/Fes family are important for hematopoeisis (*18*−*21*), but viral forms have been linked to cardiac, endothelial, and neurological disorders in transgenic mice (*22*−*24*). For members of the Fps/Fes family to have physiological effects, they must be phosphorylated on tyrosine in the kinase domain (*19*, *25*). In a previous study, we showed that removal of the single tyrosine phosphorylation site in this domain in v-Fps (pTyr-1073) lowers the rate of phosphoryl transfer by ∼2 orders of magnitude with no changes in the affinities of substrate, ATP, or Mg^{2+} (*26*). The studies presented herein show that both arginine countercharges for the activation loop phosphotyrosine are essential for autophosphorylation. However, the kinetic properties for both mutants (R1042A and R1066A) are distinct from those of the dephosphorylated v-Fps, indicating that both residues serve other functions in addition to phosphotyrosine stabilization. Interestingly, R1042A binds an inhibitor form of the substrate 12-fold better than the wild type, whereas R1066A binds the metal activator 23-fold better than the wild type. The data indicate that this protein kinase forfeits higher-affinity binding of these ligands to stabilize the activation loop, a phenomenon that provides a catalytic advantage in the phosphoryl transfer step and a means of regulation.

MATERIALS AND METHODS

Materials. Dithiothreitol (DTT), ethylenediaminetetraacetic acid, disodium salt dihydrate (EDTA), glycerol, isopropyl β-thiogalactoside (IPTG), 3-(*N*-morpholino)propanesulfonic acid (Mops), and tris(hydroxymethyl)aminomethane (Tris) were purchased from Fisher. Adenosine 5′-triphosphate (ATP), lactate dehydrogenase, type II, from bovine heart (LDH), lysozyme, nicotinamide adenine dinucleotide, reduced (NADH), phosphoenolpyruvate (PEP), and pyruvate kinase, type II, from rabbit muscle were obtained from Sigma. Cellulose resin DE52 was purchased from Whatman. Media supplies (bacto-agar, yeast extract, and tryptone peptone) were purchased from Difco. The oligonucleotides were obtained from Retrogene. DNA Mini-Prep Kits were purchased from Qiagen. The QuikChange Site-Directed Mutagenesis Kit and Epiciurian Coli XL-1 Blue cells were purchased from Stratagene. *Escherichia coli* strain BL21-(DE3) was purchased from Novagen. The plasmid vector pGEX-2T and sequencing primers pGEX 3′ and pGEX 5′ were purchased from Pharmacia.

Construction of Mutants. Mutations at Arg-1042 and Arg-1066 in the kinase domain of v-Fps were created by PCR of the entire plasmid utilizing the Stratagene QuikChange kit and an MJ Research PCT 200 Peltier thermocycler. For each mutation, a set of complementary oligonucleotides that overlap the mutation site was required. The following pairs of oligonucleotides were used for the two mutants that were studied: R1042A, 5′-AAGCACTGCATCCACGCGGAC-CTGGCTGCCCGC-3′ and 5′-TTCGTGACGTAGGTGCGC-CTGGACCGACCGGGCG-3′; and R1066A, 5′-GAGTTTGG-GATGTCGGCGCAGGAGGAGGATGGT-3′ and 5′-CTC-AAACCCTACAGCCGCGTCCTCCTCCTACCA-3′. The oligonucleotides were purified on a C-18 column and via acrylamide electrophoresis.

The PCR mixture contained 20 mM Tris-HCl (pH 8.8), 10 mM KCl, 10 mM NH_4SO_4, 2 mM $MgSO_4$, 0.1% Triton X-100, 100 μM BSA, 0.5 mM dNTP, 2.5 units of *PfuTurbo* DNA polymerase, 50−200 ng of dsDNA template, and 125 ng of each primer. The PCR cycles introduced the two base mutations during amplification of the plasmid plus the gene of interest. The PCR product was digested with 1 μL of *Dpn*I for 1 h at 37 °C to remove parental and supercoiled DNA. The purified plasmids encoding the mutation were transformed into Epicurian Coli XL-1 Blue Supercompetent cells. Purified plasmids from these clones were sequenced and subsequently transformed into the recombinant minus *E. coli* DL21(DE3) strain. Expression of the GST fusion protein was confirmed on a 13% polyacrylamide gel.

Peptides and Protein Purification. The peptide substrate, EAEIYEAIE, and inhibitor, EAEIFEAIE, were synthesized at the University of Southern California Microchemical Core Facility using Fmoc chemistry, and purified by C-18 reverse-phase HPLC. The peptides were resuspended in water, and the concentrations were determined by weight. Proteins were isolated by growing BL21(DE3) cells transformed with plasmids containing the wild-type or mutant gene. Cells were grown to an approximate OD_{600} of 0.75 in 6 L of LB medium. The cells were then induced for 2 h with 0.5 mM IPTG at room temperature, at approximately 22 °C. The cells were harvested via centrifugation, and purification of the fusion protein, GST-kin, was achieved by glutathione−agarose affinity according to previously published procedures (*27*). The total eluted protein mass, determined by the Bradford assay, was 2−4 mg for R1066A and 0.1−2 mg for R1042A. Wild-type and mutant proteins were stored at −80 °C in 50 mM Tris (pH 7.5), 1 mM EDTA, 150 mM NaCl, 1 mM DTT, and 10% glycerol. The enzymes were thawed on ice (4 °C) and used immediately for kinetic study.

Autophosphorylation of GST-kin. Approximately 30 μg of total protein was mixed with [γ-^{32}P]ATP (10 μM) and 10 mM $MgCl_2$ in a final volume of 50 μL for each mutant and the wild type. The reaction mixtures were incubated at room temperature for 30−60 min, and the reactions were stopped by adding 50 μL of 2× SDS−PAGE loading dye. The mutants and GST-kin were separated from reagents on an 8% SDS−PAGE gel. The dried gels were exposed to autoradiography film for 5 min, and the film was developed.

Radiochemical Kinetic Assays. The enzymatic activities of the enzymes were measured by monitoring the incorporation of ^{32}P into the substrate peptide from [γ-^{32}P]ATP. Typical reaction mixtures contained 10 mM free Mg^{2+}, varying levels of ATP (from 0.05 to 3 mM), 50 mM Mops (pH 7.0), 2−30 μg of R1042A or R1066A, and varying levels of EAEIYEAIE (from 0.05 to 2.4 mM) in a total volume of

50 μL. The enzyme and ATP were pre-equilbrated for approximately 5 min prior to reaction initiation. The reactions were stopped after 10 min with 26% acetic acid, and the phosphorylated peptide was separated using a DE52 cellulose column, pre-equilibrated in 30% acetic acid (*27*). All samples were collected in scintillation fluid and counted with a Beckman LS 1701 scintillation counter. Controls were performed in the absence of substrate, and the background was normally less than 5% of the reaction CPM readings.

Coupled Enzyme Assays. The activity of the wild-type enzyme was measured by spectrophotometric analysis using a coupled enzyme assay, in which ADP production is coupled with the oxidation of NADH using pyruvate kinase and lactate dehydrogenase. The reactions were manually started with varying levels of EAEIYEAIE (from 0.1 to 10 mM). The working reaction mixtures contained 50 mM Mops (pH 7.0), 0.50 mM phosphoenolpyruvate, 0.12 mM NADH, 2 units of lactate dehydrogenase, 0.5 unit of pyruvate kinase, 2 mM ATP, 12 mM $MgCl_2$, and GST-kin in a total volume of 60 μL. The rate of NADH conversion to NAD^+ was monitored at 340 nm over a time range of 45−150 s. Background reactions in the absence of peptide (taken at 0−30 s) determined that ATPase activity did not exceed 10% of the enzyme rate, and initial velocities varied linearly with protein concentration.

Viscosometric Measurements. The relative viscosities were determined using an Ostwald viscometer against a standard buffer of 50 mM Mops (pH 7.0), according to previously published procedures (*28*). The relative viscosity of each buffer was calculated using eq 1:

$$\eta^{rel} = \frac{t(\%)}{t} \times \frac{\rho(\%)}{\rho} \quad (1)$$

where η^{rel} is the relative solvent viscosity, $t(\%)$ and t are the transit times, and $\rho(\%)$ and ρ are the densities of the viscous and standard buffers, respectively. For the kinetic studies, sucrose concentrations ranging from 0 to 33% were used to provide η^{rel} values ranging from 1 to 3.4.

Modeling the Kinase Domain of v-Fps. The kinase domain of v-Fps was modeled structurally against the crystallographic coordinates of InRK (PDB entry 1ir3) using the programs Homology and Insight II (MSI). The InRK template was crystallized in the fully active trisphosphorylated form with an ATP analogue (AMP-PCP) and two divalent metals bound (*5*). The v-Fps model structure was then energy minimized for 10 000 iterations using distance-dependent dielectric constants with the program Discover (MSI).

Analysis of Data. Steady-state kinetic parameters V_{max}, $K_{peptide}$, and K_{ATP} were determined by plotting the initial reaction velocity versus either the total substrate concentration at fixed ATP concentrations or the total ATP concentration at fixed substrate peptide concentrations. The turnover rate (k_{cat}) was calculated by dividing the maximum reaction velocity (V_{max}) by the total enzyme concentration. The inhibitory parameter, K_I, was obtained by plotting the initial reaction velocity versus the total ADP concentration or the inhibitor (EAEIFEAIE) concentration at fixed ATP and substrate peptide concentrations using the following equation for competitive inhibition

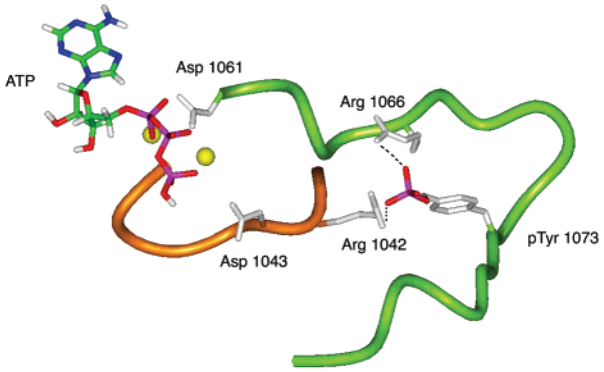

FIGURE 1: Model of the environment surrounding the phosphorylation site in the activation loop of v-Fps. This model was generated from the crystallographic coordinates of the InRK (*5*). The phosphate of Tyr-1073 forms electrostatic interactions with Arg-1042 and Arg-1066. Asp-1061 of the activation loop (green) chelates two Mg^{2+} ions (yellow spheres), while Arg-1042 is the first residue in the catalytic loop (orange) which contains the conserved Asp-1043.

$$v = \frac{V_{max}^{app}[S]}{[S] + K_m\left(1 + \frac{[I]}{K_I}\right)} \quad (2)$$

where V_{max}^{app} is V_{max} at the fixed substrate peptide or ATP concentration and K_I is the inhibitory constant for ADP or EAEIFEAIE. In the inhibition studies, S is ATP or substrate peptide and is held constant. K_m represents the K_m for either ATP or substrate peptide.

RESULTS

Model of the Activation Loop of v-Fps. Most protein kinases that are activated through activation loop phosphorylation contain two or three positively charged residues that stabilize the phosphoamino acid (*1*). While no X-ray structure for v-Fps is yet available, the structures of several homologous TPKs have been reported (*5*, *14*, *29*−*31*). The overall structures of the phosphorylated forms of these enzymes are very similar, particularly in the active site and activation loop regions. The construction of a structural model of the v-Fps kinase domain reveals two electrostatic interactions, potentially important for activity control. Figure 1 displays a model of the activation loop of v-Fps generated from the X-ray coordinates of the InRK, a TPK activated by phosphorylation (*5*). The phosphotyrosine in the activation loop of v-Fps (pTyr-1073) interacts with two charged residues: Arg-1042 and Arg-1066. The former is the first residue of the catalytic loop (RDLAARN) and is one residue away from Asp-1043. Asp-1043 is strictly conserved in all protein kinases and is likely to form a hydrogen bond with the hydroxyl of the substrate, based on X-ray data from other protein kinases (*5*, *32*, *33*). Unlike Arg-1042, Arg-1066 is part of the activation loop and is near another conserved aspartate (Asp-1061). The latter residue chelates the primary and secondary magnesium ions in the active sites of other protein kinases (*33*, *34*), thus positioning the γ-phosphate of ATP.

Autophosphorylation and Activity Profiles of the Mutants. The specific activities of the mutants and wild-type v-Fps were measured using the substrate peptide EAEIYEAIE and the radiochemical assay. As shown in Figure 2A, the specific activity of R1066A is very close to those for the autophos-

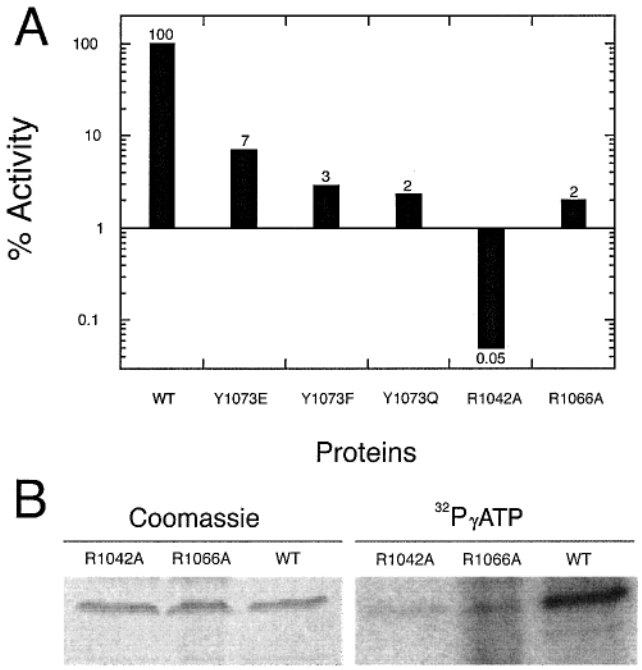

FIGURE 2: Catalytic and autophosphorylation properties of wild-type and mutant forms of v-Fps. (A) Relative specific activities of wild-type and mutant proteins. The activities of the proteins are measured using 3 mM ATP, 13 mM $MgCl_2$, and 2 mM EAEIYEAIE, and the protein concentrations are measured using a Bradford assay. The specific activities of the mutants, determined from 10 min incubations of enzyme with substrate and ATP, are displayed relative to that of the wild type which is set at 100%. The percent specific activities are also displayed numerically by the bars. The data for the Tyr-1073 mutants were taken from ref *2*. (B) Autophosphorylation of the wild type and mutants. The proteins were pre-equilibrated with [γ-^{32}P]ATP and then run on an 8% polyacrylamide gel. The Coomassie stain of the gel is shown on the left, whereas the autoradiogram of this gel is displayed on the right.

phorylation mutants and is approximately 50-fold lower than that for the phosphorylated wild-type enzyme. In comparison, the specific activity of R1042A is ~2000-fold lower than that for the wild type and 50−150-fold lower than those for the autophosphorylation mutants. Determination of whether Arg-1066 and Arg-1042 influence the phosphorylation state of Tyr-1073 in v-Fps was examined by comparing the extent of autophosphorylation in the mutant enzymes relative to that in wild-type v-Fps. Equal amounts of protein, determined with a Coomassie-stained polyacrylamide gel, were incubated with [γ-^{32}P]ATP. As shown in Figure 2B, there is a clear decrease in the extent of autophosphorylation for both R1042A and R1066A compared to that of the wild type, indicating that both residues play a significant role in the activation of v-Fps. It has been shown in previous studies that v-Fps, expressed in both bacterial and eukaryotic hosts, is autophosphorylated on a single tyrosine in the kinase domain (Tyr-1073) at a stoichiometry of approximately 0.6 mol of phosphate/mol of enzyme (*25*). The level of incorporation of ^{32}P into the two mutants is less than 10% of this amount based on densitometry readings of the autoradiogram in Figure 2B. Incubation of wild-type and mutant enzymes with and without the Mg−ATP complex for up to 30 min did not affect the specific activities, indicating that all proteins cannot be further phosphorylated within the time frame of the assays (data not shown). While wild-type v-Fps could be used potentially to phosphorylate the mutants, the specific activities of the resulting activated mutants would not be known, because of the presence of contaminating wild-type enzyme.

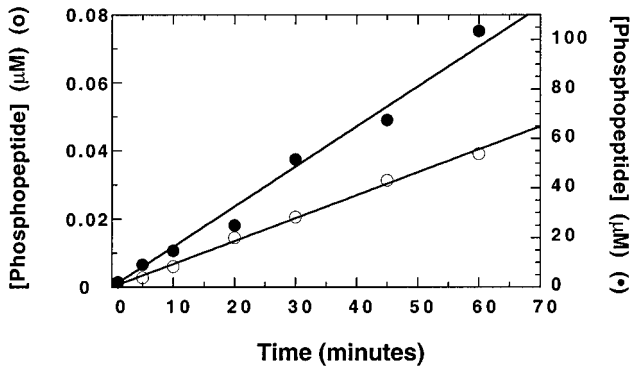

FIGURE 3: Time-dependent production of phosphopeptide for the wild type (●) and R1042 (○). Both the wild type (3 nM) and R1042A (3 nM) are mixed with 1 mM [γ-^{32}P]ATP and 1 mM substrate. The reaction is stopped with acetic acid at the designated times, and the amount of phosphopeptide is quantified using the radiochemical assay. The lines drawn through the data correspond to slope values of 1.6 μM/min and 0.67 nM/min for the wild type and R1042A, respectively.

Stability of Mutant and Wild-Type Proteins. To determine whether the low specific activities of the mutants compared to that of the wild type are due to an unstable enzyme, catalytic activity was monitored as a function of freezing and thawing and incubation time at room temperature. In a previous study, it was demonstrated that wild-type v-Fps can be stored for several months at −80 °C with no loss in catalytic activity (*3*, *35*). Likewise, both R1042A and R1066A could be stored at −80 °C for several months with no depreciation in specific activity (data not shown). Also, the mutants could be subjected to three cycles of freezing and thawing with no appreciable loss in activity (data not shown). To determine whether the mutants are subject to time-dependent inactivation during the course of experiments at room temperature, substrate phosphorylation was monitored over long time periods in excesss of normal kinetic assays. As shown in Figure 3, the extent of time-dependent phosphorylation of substrate by the wild type and R1042A, the least active mutant, is linear for up to 1 h. This is equivalent to the time range used in the autophosphorylation experiments (Figure 2B). Thus, the enzymes are stable toward low-temperature storage, do not lose activity during multiple freeze−thaw cycles, and maintain catalytic activity for 1 h at room temperature, a time frame longer than the normal assay periods.

Steady-State Kinetic and Inhibitory Parameters for Wild-Type and Mutant Enzymes. The steady-state kinetic parameters for the mutants and wild type, summarized in Table 1, were determined by varying the ATP concentration at fixed substrate peptide concentrations or by varying the substrate peptide concentration at fixed ATP concentrations. Both mutations affect the K_m for ATP (K_{ATP}) by ~2-fold relative to that of the wild type. The K_m for the substrate ($K_{peptide}$) is not significantly affected for R1042A or R1066A. The mutants lower k_{cat} by 30- and 2000-fold for R1066A and R1042A, respectively, with respect to that of the wild type. The inhibitory constants for ADP and EAEIFEAIE were measured for the mutants and wild type using the radio-

Table 1: Steady-State Kinetic Parameters for Mutant and Wild-Type Enzymes[a]

parameter	wild type	R1042A	R1066A	Y1073F[b]
k_{cat} (min^{-1})	840 ± 180	0.42 ± 0.13	26 ± 6	20
$K_{peptide}$ (mM)	0.43 ± 0.10	0.32 ± 0.08	0.37 ± 0.08	1.1
K_{ATP} (mM)	0.22 ± 0.05	0.37 ± 0.12	0.13 ± 0.02	0.25
$k_{cat}/K_{peptide}$ (mM^{-1} min^{-1})	2000 ± 600	1.3 ± 0.8	70 ± 22	18
K_I(ADP) (mM)	1.1 ± 0.15	0.69 ± 0.05	0.36 ± 0.06	
K_I(EAEIFEAIE) (mM)	4.2 ± 0.70	0.36 ± 0.036	4.2 ± 1.0	

[a] The steady-state kinetic and inhibitory parameters were measured in 50 mM Mops buffer (pH 7) using 10 mM free Mg^{2+}. The derivation of the individual constants is outlined in the text. [b] The data for the autophosphorylation mutant, Y1073F, were taken from ref *3*.

chemical assay. The enzymes were pre-equilibrated with ATP and varying amounts of the inhibitors (0−20 mM ADP or EAEIFEAIE) before reaction initiation with 0.40−2.35 mM substrate peptide. The inhibitory constants for ADP [K_I(ADP)] and EAEIFEAIE [K_I(EAEIFEAIE)] were obtained from plots of v versus increasing inhibitor concentrations using
eq 2. As summarized in Table 1, K_I(ADP) is 2−3-fold lower for R1042A and R1066A than for the wild type. The K_I(EAEIFEAIE) for R1066A is identical to that for the wild type. In contrast, the K_I(EAEIFEAIE) for R1042A is ∼12-fold lower than that for wild-type v-Fps.

Viscosity Effects on the Kinetic Parameters. The steady-state kinetic parameters k_{cat} and $k_{cat}/K_{peptide}$ for the mutants and wild type were studied as a function of varying solvent viscosity using fixed concentrations of ATP (2 mM) and $MgCl_2$ (12 mM) with varying concentrations of the substrate peptide (0.01−3.92 mM). The mutants were assayed using the radiochemical assay, while the wild-type enzyme was assayed using the coupled enzyme assay. The ratios of the steady-state kinetic parameters, k_{cat} and $k_{cat}/K_{peptide}$, in the absence and presence of sucrose [$(k_{cat})°/k_{cat}$ and $(k_{cat}/K_{peptide})°/(k_{cat}/K_{peptide})$] are shown plotted as a function of relative solvent viscosity (η^{rel}) in Figure 4. The data were fit to linear functions, and the slope values [$k_{cat}{}^{\eta}$ and $(k_{cat}/K_{peptide})^{\eta}$] are listed in Table 2. At the highest sucrose concentration (33%), the observed reaction velocities are enzyme-dependent, indicating that any rate reductions compared to 0% sucrose are not due to inhibition of the coupling agents (data not shown).

The viscosity effects on the wild-type enzyme have been interpreted previously according to the simple kinetic mechanism shown in Scheme 1 (*35*, *36*)

Scheme 1

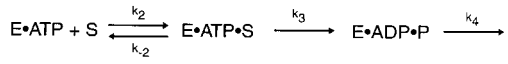

where k_2 and k_{-2} are the association and dissociation rate constants for the substrate, respectively, k_3 is rate of the phosphoryl transfer step, and k_4 is the net rate of product release. Since the k_2 and k_4 steps are bimolecular, increases in solvent viscosity are expected to lower proportionally the observed rates of these steps according to the relative viscosity of the buffer [$\eta^{rel} = k_2°k_2 = k°_{-2}/k_{-2} = k_4°/k_4$] (*37*, *38*). In comparison, the k_3 step is not expected to be influenced by solvent viscosity since it is unimolecular. It

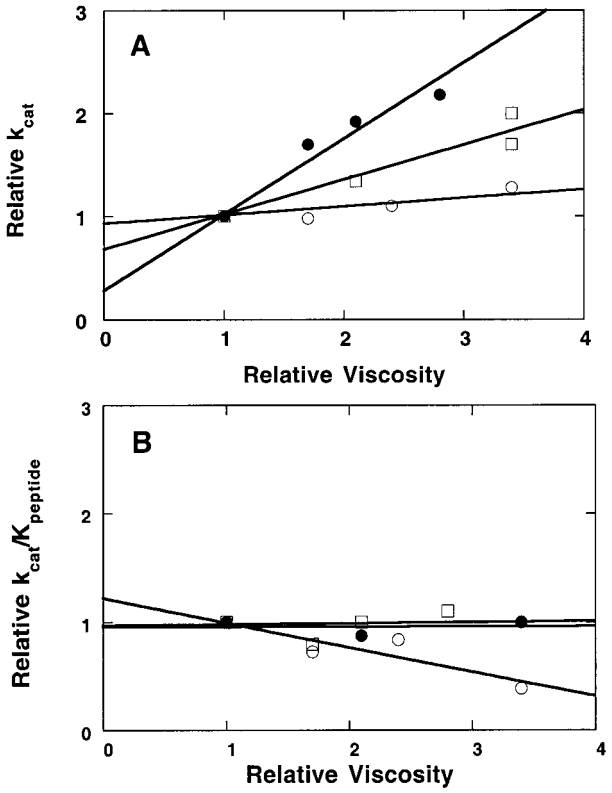

FIGURE 4: Plots of relative k_{cat} (A) and relative $k_{cat}/K_{peptide}$ (B) vs relative solvent viscosity (η^{rel}) for wild-type v-Fps (●), R1066A (○), and R1042A (□). Relative k_{cat} and relative k_{cat}/K_m are the ratios of the parameters in the absence and presence of added viscosogen [$(k_{cat})°/k_{cat}$ or $(k_{cat}/K_m)°/(k_{cat}/K_m)$]. The data are fit with line functions whose slope values are given in Table 2.

Table 2: Effects of Solvent Viscosity on the Steady-State Kinetic Parameters for Wild-Type and Mutant Enzymes[a]

parameter	wild type	R1066A	R1042A
$k_{cat}{}^{\eta}$ [b]	0.74 ± 0.04	0.06 ± 0.04	0.34 ± 0.032
$(k_{cat}/k_{peptide})^{\eta}$ [b]	0.01 ± 0.03	−0.22 ± 0.08	0.016 ± 0.054
k_3 (s^{-1})[c]	54 ± 14	0.46 ± 0.11	
k_4 (s^{-1})[c]	19 ± 4	7.2 ± 5.1	

[a] The steady-state kinetic parameters were measured in 50 mM Mops buffer (pH 7) using 10 mM free Mg^{2+} at varying percentages of sucrose. [b] The values for $k_{cat}{}^{\eta}$ and $(k_{cat}/k_{peptide})^{\eta}$ are the slopes of the linear plots in Figure 4. [c] These rate constants are determined using eqs 3 and 4 and the equation for k_{cat} derived from Scheme 1 [$k_{cat} = k_3k_4/(k_3 + k_4)$, where $k_4 = k_{cat}/k_{cat}{}^{\eta}$ and $k_3 = k_{cat}/(1 - k_{cat}{}^{\eta})$].

was shown previously that k_3 is, indeed, unaffected by solvent viscosity, whereas k_4 is sensitive to viscosogenic agents for wild-type v-Fps (*35*). The former conclusion is derived from the observation that no viscosity effect is observed on k_{cat} using poor substrates (*38*). The magnitude of the viscosity effect on k_{cat} and $k_{cat}/K_{peptide}$ can be quantified using eqs 3 and 4.

$$k_{cat}{}^{\eta} = \frac{k_3}{k_3 + k_4} \quad (3)$$

$$(k_{cat}/K_{peptide})^{\eta} = \frac{k_3}{k_{-2} + k_3} \quad (4)$$

A slope of 1 for $k_{cat}{}^{\eta}$ and $(k_{cat}/K_{peptide})^{\eta}$ implies that the rate of phosphoryl transfer is faster than that of net product release

and the dissociation rate for the substrate ($k_{-2} < k_3 > k_4$). In contrast, the absence of viscosity effects on either steady-state kinetic parameter is consistent with slow phosphoryl transfer compared to the other steps in the reaction scheme ($k_{-2} > k_3 < k_4$).

An intermediate value for k_{cat}^{η} is obtained for the wild type and is consistent with partial rate limitation by k_3 and k_4 (Table 2). In comparison, no significant viscosity effect is observed on k_{cat} for R1066A, an effect that is consistent with rate-limiting phosphoryl transfer (i.e., $k_3 \ll k_4$). A switch in the kinetic mechanism from partially rate-limiting phosphoryl transfer to rate-limiting phosphoryl transfer has been observed previously for several mutants of v-Fps (*3*, *28*, *36*). In general, mutants with very low values for k_{cat} compared to that of the wild type are expected to display blunted viscosity effects on this parameter. Such a result supports the interpretation of the kinetic mechanism in Scheme 1 for the mutants. Wild-type v-Fps displays no viscosity effect on $k_{cat}/K_{peptide}$, a result which implies that the substrate is in rapid exchange with the active site (i.e., $k_3 \ll k_{-2}$). In contrast to this simple model for the wild type, a large viscosity effect is observed on k_{cat} for R1042A, although this parameter is considerably lower than the values for R1066A and the wild type. Also, viscosogenic agents increase $k_{cat}/K_{peptide}$ for R1066A, an effect that is not consistent with the original presumptions applied to the model depicted in Scheme 1. These issues will be considered further in the Discussion.

Effects of Free Magnesium on Reaction Velocity. Increasing the free concentration of Mg^{2+} potently activates the catalytic activity of wild-type v-Fps because of the increased occupancy of a second metal binding site in the nucleotide pocket (*26*). The primary metal binds as an ATP−Mg complex so that changes in the level of free Mg^{2+} measures the level of binding to the second site. The effects of arginine-to-alanine mutations on the affinity of this second Mg^{2+} ion in the active site were examined by plotting v versus increasing free Mg^{2+} concentrations (from 0.25 to 50 mM free) at fixed peptide (2.35 mM) and ATP (2 mM) concentrations. The relative velocities of the mutants and wild type are displayed in Figure 5. The data are fit to hyperbolic functions to obtain dissociation constants for Mg^{2+} (K_{Mg}) of 16 ± 1, 12 ± 2, and 0.70 ± 0.02 mM for the wild type, R1042A, and R1066A, respectively. For the mutants, the initial velocity extrapolates to a near-zero value at zero free metal ion concentration. For the wild type, however, a non-zero intercept, which is 12-fold lower than the maximum rate, is attained at zero free metal. This is consistent with previous findings for the wild-type enzyme (*26*). We presume that the extrapolation to near-zero initial velocity for R1042A and R1066A does not necessarily imply that these mutants are not active in the absence of the second metal ion. Rather, it is difficult to measure these rates for the low-activity mutants at low concentrations of free Mg^{2+} (i.e., <0.5 mM). Furthermore, the reaction velocity for R1066A increases sharply at low, free Mg^{2+} concentrations, making it difficult to attain an accurate y-intercept determination.

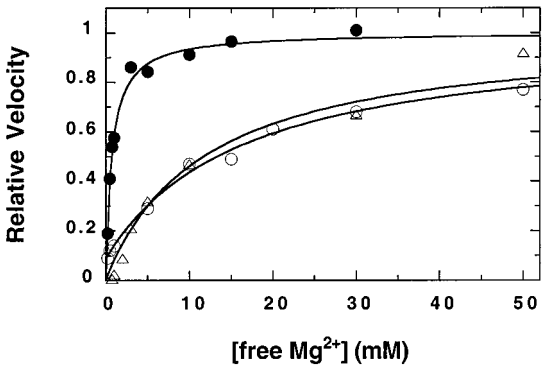

FIGURE 5: Effects of free Mg^{2+} on the activation of wild-type v-Fps (○), R1042A (△), and R1066A (●). Enzymes are pre-equilibrated with ATP (2 mM) and varying free concentrations of Mg^{2+} (from 0.5 to 50 mM) prior to initiation of the reaction with 2.4 mM EAEIYEAEI. The initial velocities (v) are normalized to the velocities attained at infinite free Mg^{2+} derived from hyperbolic fitting. The apparent affinities of Mg^{2+} (K_{Mg}) are 16 ± 1, 12 ± 2, and 0.70 ± 0.03 mM for the wild type, R1042A, and R1066A, respectively. The wild-type value is fit to a non-zero y-intercept that is 12-fold lower than the maximum rate at an infinite free Mg^{2+} concentration.

DISCUSSION

The upregulation of protein kinases through activation loop phosphorylation is associated with a number of conformational changes detected using X-ray crystallographic methods (*1*). Some of these motions have been observed in solution using hydrogen−deuterium exchange studies (*39*, *40*). In this study, the function of two electropositive residues, positioned to stabilize the activation loop phosphotyrosine in the oncoprotein v-Fps, was studied in a solution setting. The goal is to determine whether Arg-1042 and Arg-1066 (Figure 1) function solely as rigid anchors for the phosphotyrosine or whether they serve other functions not readily apparent in the crystallographic models. In the former case, it is expected that removal of the arginines would produce mutants with kinetic profiles similar to those for the dephosphorylated, repressed enzyme. Since wild-type v-Fps readily autophosphorylates in vitro, we can mimic the repressed state with mutants at Tyr-1073 (Y1073F, -Q, and -E) and use the biophysical parameters of these proteins to set the basal activity level prior to activation. If the electropositive residues serve other functions, altered biophysical parameters might reveal insights into how the phosphotyrosine in the loop regulates the phosphoryl transfer reaction from a distal location. While v-Fps is oncogenic, there are no differences in the kinase domains of the viral and cellular forms so that these studies may be largely applied to other members of the Fps/Fes family. Both arginines are essential for high-level autophosphorylation since either mutation leads to enzymes with poor autophosphorylation properties (Figure 2B). Initial crude activity assays suggest that Arg-1066 functions only to stabilize the phosphotyrosine since removal of this residue in R1066A leads to a catalytic activity similar to those for the autophosphorylation mutants. In comparison, the specific activity of R1042A is almost 2 orders of magnitude lower than those of Y1073Q and Y1073F (Figure 2A), suggesting that this residue serves other functions in the kinase domain.

Effects of Arginine Replacement on the Phosphoryl Transfer Rate. To attain a more informed understanding of the effects of the arginine-to-alanine substitutions in v-Fps, steady-state kinetic parameters for R1042A and R1066A were determined and compared to those of Y1073F, a mutant that represents the repressed form of the enzyme. Consistent with the specific activity measurements, the turnover number

for R1066A is similar to that for Y1073F while that for R1042A is approximately 2 orders of magnitude lower (Table 1). For R1066A, the 30-fold decrease in k_{cat} relative to that of the wild type is due to a 100-fold decrease in the rate of phosphoryl transfer (Table 2). This decrease is similar to that observed for the autophosphorylation mutants, further strengthening the role of Arg-1066 as a rigid electropositive anchor for phosphotyrosine (*3*). The assessment of the phosphoryl transfer rate relies upon the measurement of k_{cat} and, thus, the active enzyme concentration. Two important observations indicate that the k_{cat} effect on R1066A is not due to an inactive enzyme. First, increased viscosity does not affect k_{cat} for R1042A relative to the wild type (Table 2). If mutation partitions the enzyme between inactive and active forms through changes in protein stability, a wild-type-like viscosity effect would be anticipated since $k_{cat}\eta$ is a relative parameter and has no enzyme dependence. This criterion has been applied to other mutants of v-Fps (*3*, *28*, *36*) and the nonreceptor TPK, Csk (*41*), and the dephosphorylated forms of the InRK (*13*) and Cdk2 (*4*). Moreover, the disappearance of a viscosity effect is a standard control for the correct interpretation of enzyme viscosometric studies (*37*). Second, the mutation at Arg-1066 causes changes in the affinity of the activating metal ion, Mg^{2+}, which is not dependent upon enzyme concentration (Figure 5).

While R1042A displays a lower k_{cat} than R1066A (Table 1), a measurable viscosity effect is observed on this parameter (Table 2). This effect is not consistent with a simple phosphorylation mechanism in which the catalytic step is limited solely by phosphoryl transfer as expected for a mutant bearing a low k_{cat}. Nonetheless, the k_{cat} effect for replacement at Arg-1042 is not likely to result from an inactive enzyme for three reasons. First, the enzyme is stable under all storage and assay conditions for the experiments (Figure 3). If the mutant destabilized the enzyme, time-dependent inactivation would be expected. Second, the viscosity effect on k_{cat} is intermediate between those of R1066A and the wild type. If the overall effect of the mutation is to generate large amounts of inactive enzyme, a change in the kinetic mechanism, as evidenced by the altered viscosity effect, would not be expected. Third, mutation at Arg-1042 influences peptide binding, a parameter that is independent of active enzyme concentration (Table 1). The viscosity effect on R1042A can be explained if a large, slow conformational step limits k_{cat}. Large viscosity effects on poorly active mutants of triosephosphate isomerase have been reported and accordingly linked to movements in an active site loop (*42*). Because of the position of Arg-1042 in the active site (Figure 1), it is conceivable that the arginine controls vital motions in the catalytic loop such that mutation impairs fast attainment of a productive form. Such an event would expand the kinetic mechanism in Scheme 1 to include a slow conformational change that might precede the phosphoryl transfer step. In further support of this model, mutation of the conserved aspartate (D149N) in the catalytic loop of phosphorylase kinase, an enzyme that does not require activation loop phosphorylation, leads to a 3 orders of magnitude decrease in k_{cat}, yet the protein is fully folded and exhibits a large viscosity effect on this parameter (*43*). Because of the location of this residue in the catalytic loop, the latter solvent effect could be related to the proposed slow conformational change.

Phosphotyrosine Countercharges Influence Ligand Affinity. While the mutations do not impact K_{ATP} or $K_{peptide}$ by more than 2-fold, these observations do not imply that the true affinities of peptide and nucleotide are unaffected. Apparent affinity constants are complex terms that may involve the mathematical inclusion of all the forward and reverse steps in the kinetic mechanism. For example, the K_d for a substrate peptide (LRRASLG) bound to PKA is ~2 orders of magnitude higher than $K_{peptide}$ because of a rapid phosphoryl transfer rate and a slow net release rate for products (*44*). Viscosity studies can be used to estimate K_d values (*28*, *36*), but in the study presented here, R1042A does not conform to the simple kinetic mechanism in Scheme 1 because of the large viscosity effect on turnover (Table 2). Given these limitations, inhibitor studies were used to determine the affinities of various ligands in the active sites of the mutants. Unlike K_m measurements, by definition, K_I values reflect true affinity constants for a ligand and an enzyme. Both mutations have effects of 2−3-fold on ADP binding, while the affinity of the inhibitor peptide toward R1066A is unaffected relative to the wild type. Surprisingly, the affinity of the inhibitor peptide is enhanced by 12-fold by the removal of Arg-1042 (Table 1). This unusual finding is not predicted by the model in Figure 1 or the X-ray structures of other protein kinases. On the basis of these data, we conclude that the arginine in the catalytic loop of v-Fps destabilizes the binding of substrate. While this conclusion is inferred from inhibitor studies, it is likely that this applies to substrates as well since the inhibitor only differs from the substrate by a phosphorylatable hydroxyl, binds with an affinity similar to that of the substrate, and is purely competitive with the substrate (*35*).

Selective Effects on the Metal Activator. The phosphotyrosine in the activation loop of v-Fps activates the kinase domain by enhancing the rate of phosphoryl transfer by 2 orders of magnitude without affecting ligand affinity (*3*). Thus, stabilization of this residue through carefully positioned countercharges is essential for high catalytic throughput. Whether these electropositive residues serve other functions has been unclear, until now. The data for R1066A are consistent with the simple, localized function of phosphotyrosine stabilization since the steady-state kinetic parameters are close to those for the autophosphorylation mutants (Table 1 and Figure 2). However, a closer look at the activation parameters of this mutant reveals a surprising role for Arg-1066. Wild-type v-Fps is strongly activated by Mg^{2+} concentrations that are in excess of the ATP concentration because of the binding of a second metal ion in the active site (*26*). Since Arg-1066A is close to the conserved Asp-1061, which chelates the metal ions (Figure 1), we wondered whether this positively charged residue could individually serve the auxiliary function of modulating metal ion binding. Although R1042A binds Mg^{2+} with a K_{Mg} close in value to that for the wild type, surprisingly R1066A binds Mg^{2+} 23-fold *better* than the wild type (Figure 5). These results have not been observed for any of the autophosphorylation mutants (*3*), suggesting that Arg-1066 serves the unique function of destabilizing the binding of one of the active site metal ions. Also, these observations, like those derived from the inhibitor affinity studies in the previous section (Table 1), are predicated upon protein-independent parameters and, thus, do not vary with the active enzyme concentration.

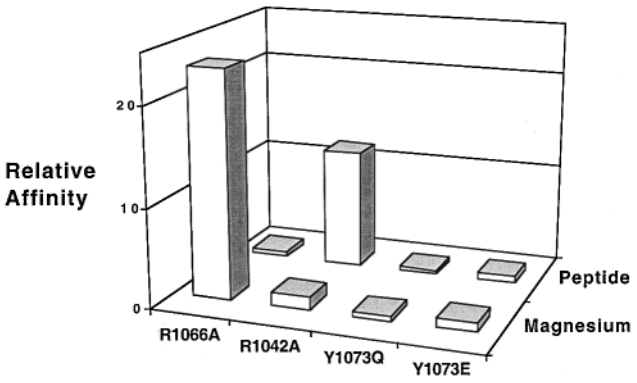

FIGURE 6: Relative binding affinities of magnesium and peptide inhibitor to wild-type and mutant enzymes. Relative affinity is expressed as the ratio of the dissociation constants for the inhibitor (K_I) or magnesium (K_{Mg}) relative to the wild-type v-Fps parameters. Values of >1 imply that the ligand displays improved affinity relative to the wild type. The data for the wild type, R1042A, and R1066A are taken from Table 1, whereas the data for Y1073E and Y1073Q are taken from ref *3*.

General Principles for Electrostatic Stabilization of the Activation Loop in Fps-Related Enzymes. The introduction of arginine-to-alanine replacements in v-Fps permits us to derive some general principles for phosphorylation-driven activation that could be applied to other members of the Fps/Fes protein kinase family. First, phosphorylation of the activation loop and its stabilization by electropositive residues does not enhance substrate or nucleotide binding. These results support the notion that the activation loop in v-Fps is not an autoinhibitor as proposed for the InRK (*5*) and Cdk2 (*7*). Second, both electrostatic contacts (Arg-1042 and Arg-1066) are essential for high catalytic activity and phosphotyrosine stabilization. Third, both arginines serve discrete functions for substrate phosphorylation beyond phosphotyrosine stabilization. As shown in Figure 6, R1042A uniquely affects peptide binding without influencing Mg^{2+} binding. In contrast, R1066A does not influence peptide binding but uniquely increases the affinity of Mg^{2+}. These findings indicate that the electrostatic stabilization of the activation loop is attained at the expense of high substrate and activating metal ion affinities. This is reminiscent of the Circe effect in which an enzyme residue or ensemble of residues induces strain in the substrate to better facilitate formation of the reaction transition state (*45*, *46*). While the data presented herein are derived from mutants which mimic the repressed form of v-Fps (i.e., unphosphorylated at Tyr-1073), there is no evidence that activation loop phosphorylation relieves this strain. The binding affinities of substrate and metal are the same in both the phosphorylated and dephosphorylated (Y1073Q and -E, respectively) enzyme forms and are both lower than those for R1042A and R1066A (Figure 6). As predicted, this strain is only relieved in the reaction transition state (*45*, *46*). At this time, it is unclear how the electropositive centers specifically induce strain in the active site. Whatever the molecular cause, however, the data suggest that v-Fps and possibly other protein kinases limit the maximum binding potential in the active site in place of a fast phosphoryl transfer step that can be regulated through loop phosphorylation.

ACKNOWLEDGMENT

We thank Dr. Patricia Jennings for helpful insights and for carefully reviewing the manuscript.

REFERENCES

1. Johnson, L. N., Noble, M. E., and Owen, D. J. (1996) *Cell 85*, 149−158.
2. Adams, J. A., McGlone, M. L., Gibson, R., and Taylor, S. S. (1995) *Biochemistry 34*, 2447−2454.
3. Saylor, P., Hanna, E., and Adams, J. A. (1998) *Biochemistry 37*, 17875−17881.
4. Hagopian, J. C., Kirtley, M. P., Stevenson, L. M., Gergis, R. M., Russo, A. A., Pavletich, N. P., Parsons, S. M., and Lew, J. (2001) *J. Biol. Chem. 276*, 275−280.
5. Hubbard, S. R. (1997) *EMBO J. 16*, 5572−5581.
6. Canagarajah, B. J., Khokhlatchev, A., Cobb, M. H., and Goldsmith, E. J. (1997) *Cell 90*, 859−869.
7. Jeffrey, P. D., Russo, A. A., Polyak, K., Gibbs, E., Hurwitz, J., Massague, J., and Pavletich, N. P. (1995) *Nature 376*, 313−320.
8. Knighton, D. R., Zheng, J. H., Ten Eyck, L. F., Xuong, N. H., Taylor, S. S., and Sowadski, J. M. (1991) *Science 253*, 414−420.
9. Knighton, D. R., Zheng, J. H., Ten Eyck, L. F., Ashford, V. A., Xuong, N. H., Taylor, S. S., and Sowadski, J. M. (1991) *Science 253*, 407−414.
10. Hubbard, S. R., Wei, L., Ellis, L., and Hendrickson, W. A. (1994) *Nature 372*, 746−754.
11. Russo, A. A., Jeffrey, P. D., and Pavletich, N. P. (1996) *Nat. Struct. Biol. 3*, 696−700.
12. Zhang, F., Strand, A., Robbins, D., Cobb, M. H., and Goldsmith, E. J. (1994) *Nature 367*, 704−711.
13. Ablooglu, A. J., and Kohanski, R. A. (2001) *Biochemistry 40*, 504−513.
14. Yamaguchi, H., and Hendrickson, W. A. (1996) *Nature 384*, 484−489.
15. Pawson, T., Guyden, J., Kung, T. H., Radke, K., Gilmore, T., and Martin, G. S. (1980) *Cell 22*, 767−775.
16. Feldman, R. A., Hanafusa, T., and Hanafusa, H. (1980) *Cell 22*, 757−765.
17. Hanafusa, T., Wang, L. H., Anderson, S. M., Karess, R. E., Hayward, W. S., and Hanafusa, H. (1980) *Proc. Natl. Acad. Sci. U.S.A. 77*, 3009−3013.
18. Feldman, R. A., Gabrilove, J. L., Tam, J. P., Moore, M. A., and Hanafusa, H. (1985) *Proc. Natl. Acad. Sci. U.S.A. 82*, 2379−2383.
19. Fang, F., Ahmad, S., Lei, J., Klecker, R. W., Trepel, J. B., Smithgall, T. E., and Glazer, R. I. (1993) *Biochemistry 32*, 6995−7001.
20. Smithgall, T. E., Yu, G., and Glazer, R. I. (1988) *J. Biol. Chem. 263*, 15050−15055.
21. Yu, G., Smithgall, T. E., and Glazer, R. I. (1989) *J. Biol. Chem. 264*, 10276−10281.
22. Greer, P., Haigh, J., Mbamalu, G., Khoo, W., Bernstein, A., and Pawson, T. (1994) *Mol. Cell. Biol. 14*, 6755−6763.
23. Yee, S. P., Mock, D., Greer, P., Maltby, V., Rossant, J., Bernstein, A., and Pawson, T. (1989) *Mol. Cell. Biol. 9*, 5491−5499.
24. Yee, S. P., Mock, D., Maltby, V., Silver, M., Rossant, J., Bernstein, A., and Pawson, T. (1989) *Proc. Natl. Acad. Sci. U.S.A. 86*, 5873−5877.
25. Weinmaster, G., Zoller, M. J., Smith, M., Hinze, E., and Pawson, T. (1984) *Cell 37*, 559−568.
26. Saylor, P., Wang, C., Hirai, T. J., and Adams, J. A. (1998) *Biochemistry 37*, 12624−12630.
27. Gish, G., McGlone, M. L., Pawson, T., and Adams, J. A. (1995) *Protein Eng. 8*, 609−614.
28. Konkol, L., Hirai, T. J., and Adams, J. A. (2000) *Biochemistry 39*, 255−262.
29. Schindler, T., Sicheri, F., Pico, A., Gazit, A., Levitzki, A., and Kuriyan, J. (1999) *Mol. Cell 3*, 639−648.

30. Lamers, M. B., Antson, A. A., Hubbard, R. E., Scott, R. K., and Williams, D. H. (1999) *J. Mol. Biol. 285*, 713−725.
31. Mohammadi, M., Schlessinger, J., and Hubbard, S. R. (1996) *Cell 86*, 577−587.
32. Madhusudan, Trafny, E. A., Xuong, N. H., Adams, J. A., Ten Eyck, L. F., Taylor, S. S., and Sowadski, J. M. (1994) *Protein Sci. 3*, 176−187.
33. Owen, D. J., Noble, M. E., Garman, E. F., Papageorgiou, A. C., and Johnson, L. N. (1995) *Structure 3*, 467−482.
34. Zheng, J., Knighton, D. R., Ten Eyck, L. F., Karlsson, R., Xuong, N., Taylor, S. S., and Sowadski, J. M. (1993) *Biochemistry 32*, 2154−2161.
35. Wang, C., Lee, T. R., Lawrence, D. S., and Adams, J. A. (1996) *Biochemistry 35*, 1533−1539.
36. Hirai, T. J., Tsigelny, I., and Adams, J. A. (2000) *Biochemistry 39*, 13276−13284.
37. Brouwer, A. C., and Kirsch, J. F. (1982) *Biochemistry 21*, 1302−1307.
38. Adams, J. A., and Taylor, S. S. (1992) *Biochemistry 31*, 8516−8522.
39. Hoofnagle, A. N., Resing, K. A., Goldsmith, E. J., and Ahn, N. G. (2001) *Proc. Natl. Acad. Sci. U.S.A. 98*, 956−961.
40. Andersen, M. D., Shaffer, J., Jennings, P. A., and Adams, J. A. (2001) *J. Biol. Chem. 276*, 14204−14211.
41. Sondhi, D., and Cole, P. A. (1999) *Biochemistry 38*, 11147−11155.
42. Sampson, N. S., and Knowles, J. R. (1992) *Biochemistry 31*, 8488−8494.
43. Skamnaki, V. T., Owen, D. J., Noble, M. E., Lowe, E. D., Lowe, G., Oikonomakos, N. G., and Johnson, L. N. (1999) *Biochemistry 38*, 14718−14730.
44. Grant, B. D., and Adams, J. A. (1996) *Biochemistry 35*, 2022−2029.
45. Jencks, W. P. (1975) *Adv. Enzymol. Relat. Areas Mol. Biol. 43*, 219−410.
46. Toney, M. D., and Kirsch, J. F. (1993) *Biochemistry 32*, 1471−1479.

BI010838E